Earth and Planetary Science Letters 621 (2023) 118371

Contents lists available at ScienceDirect

Earth and Planetary Science Letters

journal homepage: www.elsevier.com/locate/epsl

Cadmium isotopic evidence for reduced deep-water marine primary productivity during the end-Permian mass extinction

Yuxu Zhang [a], Hanjie Wen [b,a,c,*], Haifeng Fan [a], Chuanwei Zhu [a], Jiafei Xiao [a], Pan Qiao [a,c]

[a] State Key Laboratory of Ore Deposit Geochemistry, Institute of Geochemistry, Chinese Academy of Sciences, Guiyang 550081, China
[b] School of Earth Sciences and Resources, Chang'an University, Xi'an 710054, China
[c] College of Earth and Planetary Sciences, University of Chinese Academy of Sciences, Beijing 100049, China

ARTICLE INFO

Article history:
Received 21 March 2023
Received in revised form 22 August 2023
Accepted 27 August 2023
Available online 15 September 2023
Editor: L. Coogan

Keywords:
Cd isotopes
primary productivity
end-Permian mass extinction
South China

ABSTRACT

Marine primary productivity is a key control on the stability of marine ecosystems. Decreasing marine primary productivity might have led to the end-Permian mass extinction, although this is debated. However, the changes in primary productivity at different seawater depths during the end-Permian mass extinction remain poorly constrained. We investigated the Cd isotopic systematics of shallow-water (Dajiang) and deep-water (Shangsi) sedimentary sections in South China. Combined with previously published data from an intermediate–deep-water section (Meishan), we were able to reconstruct the depth changes in marine primary productivity. In the Dajiang section, prior to the mass extinction, the Cd isotopic compositions of seawater ($\delta^{114/110}Cd_{SW}$) varied from +0.73‰ to +0.92‰, with an average of +0.83‰ ± 0.13‰ (2SD; n = 11). During and after the mass extinction, $\delta^{114/110}Cd_{SW}$ varied from +0.73‰ to +0.91‰, with an average of +0.81‰ ± 0.12‰ (2SD; n = 12). In the Shangsi and Meishan sections, prior to the mass extinction, $\delta^{114/110}Cd_{SW}$ varied from +0.47‰ to +0.85‰, with an average of +0.66‰ ± 0.16‰ (2SD; n = 35). During and after the mass extinction, $\delta^{114/110}Cd_{SW}$ varied from −0.19‰ to +0.36‰, with an average of −0.02‰ ± 0.27‰ (2SD; n = 27). During the end-Permian mass extinction, the marine primary productivity recorded by Cd isotopes in the relatively deep-water sections was considerably reduced, which may have caused the destruction of relatively deep-water marine ecosystems. We suggest that upward expansion of sulfidic and anoxic deep water, possibly due to the volcanic eruption of the Siberian Traps large igneous province, was one of the causes of the decrease in marine primary productivity. However, the marine primary productivity did not change in the shallow-water section during the end-Permian mass extinction, although changes in the types of marine primary producers are evident from the fossil record. This change in the types of primary producers may have contributed to the mass extinction in shallow-water platform environments. Vertical variations in the changes in primary productivity indicate that the environmental factors leading to the extinction event mainly began in deep waters during the end-Permian mass extinction.

1. Introduction

The end-Permian mass extinction was the most severe biotic crisis in the Phanerozoic. Over 81% of marine species became extinct, resulting in the destruction of marine ecosystems (Fan et al., 2020). Previous studies have proposed several hypotheses to explain this mass extinction, including volcanic eruptions (e.g., Burgess et al., 2017; Liu et al., 2017; Shen et al., 2019; Zhang et al., 2021), anoxic events (e.g., Grice et al., 2005; Shen et al., 2011; F.F. Zhang, Shen et al., 2020), and ocean acidification (e.g., Garbelli et al., 2017; Jurikova et al., 2020), but its cause remains controversial. The productivity of primary producers at the bottom of the food chain is a fundamental factor in maintaining the stability of marine ecosystems (e.g., Field et al., 1998) and plays a key role in regulating local and global C cycles (e.g., Farmer et al., 2021; Horner et al., 2021). Changes in primary productivity may link continental weathering to marine redox changes (e.g., Ge and Bond, 2022). Therefore, reconstruction of the marine primary productivity during the Permian–Triassic (P–T) transition may be a useful approach for investigating this extinction event. However, previous studies of the marine primary productivity during the P–T transition have resulted in two diametrically opposed hypotheses. One is that the primary productivity of the oceans decreased during the mass extinction period

* Corresponding author at: School of Earth Sciences and Resources, Chang'an University, Xi'an 710054, China.
E-mail address: wenhanjie@vip.gyig.ac.cn (H. Wen).

https://doi.org/10.1016/j.epsl.2023.118371
0012-821X/

(e.g., Grasby et al., 2016; Zhang et al., 2018; Ge and Bond, 2022), whereas the other is that the marine primary productivity increased (e.g., Meyer et al., 2011; Shen et al., 2015; Qiu et al., 2019). In addition, during the P–T transition, microbialites were extensively deposited in several shallow-water platform settings worldwide, but no microbialite deposits are known to have formed in relatively deep-water settings at this time. Microbialite deposition almost coincided with the mass extinction event (e.g., Wang et al., 2005; Wu et al., 2016; X.Y. Zhang, Zheng et al., 2020), and abundant infaunal metazoan fossils occur in the microbialites (e.g., Forel, 2013; Yang et al., 2015; Martindale et al., 2019). This implies that changes in primary productivity at different water depths were variable before/after the mass extinction. Unfortunately, the vertical changes in the primary productivity are unclear.

Nutrient elements (e.g., N, P, Si, Fe, Mn, and Zn) in ancient seawater were necessary for the survival of primary producer organisms at the base of the food chain, and have played a key role in the evolution of life throughout geological history (e.g., Tyrrell, 1999; Paytan and Mclaughlin, 2007; Farmer et al., 2021). The distribution and changes in nutrient element concentrations in the ocean can constrain nutrient utilization and primary productivity. Cadmium is also a micronutrient for microorganisms and is involved in some critical enzymes in marine phytoplankton (e.g., Lane et al., 2005; Abouchami et al., 2014). In the modern ocean, the dissolved Cd and phosphate have a similar distribution along a depth gradient, with low concentrations in surface waters, increasing concentrations with depth, and fairly constant concentrations in deep waters ($>$ 1000 m). This is due to the removal of both elements by phytoplankton from surface waters and re-mineralization of sinking organic debris at depth (e.g., Boyle et al., 1976; de Baar et al., 1994; Ripperger et al., 2007). Culturing experiments have demonstrated that phytoplankton preferentially uptake light Cd isotopes, resulting in residual seawater being relatively enriched in heavy Cd isotopes (Lacan et al., 2006). The Cd isotopic composition of modern seawater exhibits significant variability, with a nearly uniform deep-ocean ($>$ 1000 m) $\delta^{114/110}$Cd value of $\sim$ 0.2‰, and $\delta^{114/110}$Cd values of 0.6‰–1.0‰ in surface waters, which is attributed to kinetic isotopic effects resulting from the preferential uptake of lighter Cd isotopes by phytoplankton (e.g., Lacan et al., 2006; Ripperger et al., 2007; Abouchami et al., 2011, 2014; Xue et al., 2013; Conway and John, 2015; George et al., 2019; Sieber et al., 2019). Therefore, seawater Cd isotopic compositions can be used to trace changes in nutrient utilization, and a high $\delta^{114/110}$Cd value indicates a relatively high nutrient utilization (e.g., Georgiev et al., 2015; Horner et al., 2021). If the Cd supply can be adequately constrained, the seawater $\delta^{114/110}$Cd values can be used to trace marine primary productivity (e.g., Horner et al., 2021).

Both Cd and P are estimated to have similar oceanic residence times of 10–100 kyr (Bewers and Yeats, 1977; Ripperger and Rehkämper, 2007). Cadmium in seawater can replace Ca in marine carbonate rocks and be well preserved in such lithologies (e.g., Tesoriero and Pankow, 1996; Horner et al., 2011). Experiments have shown that the Cd isotopic fractionation factor ($\alpha_{CaCO3-Cd(aq)}$) during calcite precipitation in seawater is 0.99955 $\pm$ 0.00012, and that it is not affected by temperature or the $CaCO_3$ precipitation rate (Horner et al., 2011). Based on estimates of the Cd flux in the modern ocean, and given the amount of Cd entering $CaCO_3$ is low, the incorporation of Cd into $CaCO_3$ has almost no effect on the Cd isotopic composition of seawater as compared with the Cd uptake by phytoplankton (Horner et al., 2011). Therefore, marine carbonates can record the Cd isotopic composition of seawater and be used to study changes in nutrient utilization and marine primary productivity. Several studies have confirmed that the Cd isotopic composition of paleo-seawater is recorded by both old and young carbonate strata (e.g., Ediacaran–Cambrian, upper Permian, and Holocene strata) (John et al., 2017; Zhang et al., 2018; Druce et al., 2022; Frederiksen et al., 2022).

To constrain the nutrient utilization and primary productivity at different seawater depths during the end-Permian mass extinction, we investigated the Cd isotopic systematics of shallow- and deep-water sections in South China. These include the Dajiang section (water depths $<$ 20 $-$ 30 m; Lehrmann et al., 1998) and Shangsi section (water depths = 150 $-$ 200 m; Godbold et al., 2017; Zheng et al., 2022). Combined with previously published data from the intermediate–deep-water Meishan section (water depths = 50 $-$ 100 m; Yin et al., 2001; Lei et al., 2019), we reconstructed the marine primary productivity at different seawater depths in the Paleo-Tethys Ocean.

2. Geological setting

In the Permian, the South China Block was an independent island located in the Paleo-Tethys Ocean (Fig. 1a). During the P–T transition, the South China Block had a paleogeography consisting of the Yangtze carbonate platform in its central, western, and eastern (in the present-day orientation) regions that transitioned from continental to marine–continental transitional facies, and southern and northern margins that were deep-water basin facies (Yin et al., 2014) (Fig. 1b). The Nanpanjiang Basin was located at the southern margin of the Yangtze Platform, and the isolated carbonate platform in the northern Nanpanjiang Basin is called the Great Bank of Guizhou (Lehrmann et al., 1998). The Dajiang section is located in the Great Bank of Guizhou and contains shallow-water platform sediments (water depths $<$ 20 $-$ 30 m; Lehrmann et al., 1998) (Fig. 1b). Both the Shangsi and Meishan sections are located along the northern margin of the Yangtze Platform. The Shangsi section was deposited in the lower slope environment of a deep platform margin (water depths = 150 $-$ 200 m; Godbold et al., 2017; Zheng et al., 2022), while the Meishan section was deposited in the upper slope environment of a platform margin (water depths = 50 $-$ 100 m; Yin et al., 2001; Lei et al., 2019) (Fig. 1b). The Meishan section has been defined as a Global Stratotype Section and Point of the Permian–Triassic Boundary (Yin et al., 2001).

3. Samples and methods

Samples were collected from the three P–T sections, including 23 samples from the Dajiang section, 21 samples from the Shangsi section, and 42 samples from the Meishan section. All samples were freshly exposed. Prior to geochemical analysis, each sample was cleaned with deionized water and dried, and then crushed to $<$ 200 mesh (0.074 mm). All the acids used in this study were purified by sub-boiling distillation, and the water used was 18.2 MΩ grade obtained from a Millipore system.

Major and trace elements were analyzed with an inductively coupled plasma–optical emission spectrometer (ICP–OES; Varian Vista MPX) and ICP–mass spectrometer (ICP–MS; PE ELAN DRC-e), respectively, at the State Key Laboratory of Ore Deposit Geochemistry (SKLODG), Institute of Geochemistry, Chinese Academy of Sciences, Guiyang, China. The analytical uncertainty of the elemental concentrations is generally less than ±10%. Sequential extraction using acetic acid was employed to separate the carbonate-phase Cd from the samples, and the analytical methodology is described in detail in the Supplementary Material.

The $\delta^{114/110}$Cd values of the Meishan section samples were taken from Zhang et al. (2018). For the Dajiang and Shangsi sections, after determining the Cd contents, powdered sub-samples containing $\sim$ 0.10 μg of Cd were placed in a glass funnel and then cleaned with deionized water and 1 M ammonium acetate to elute exchangeable Cd. Samples were transferred to 100 mL beakers, and 40 mL of 1 M acetic acid was slowly added to digest the samples.

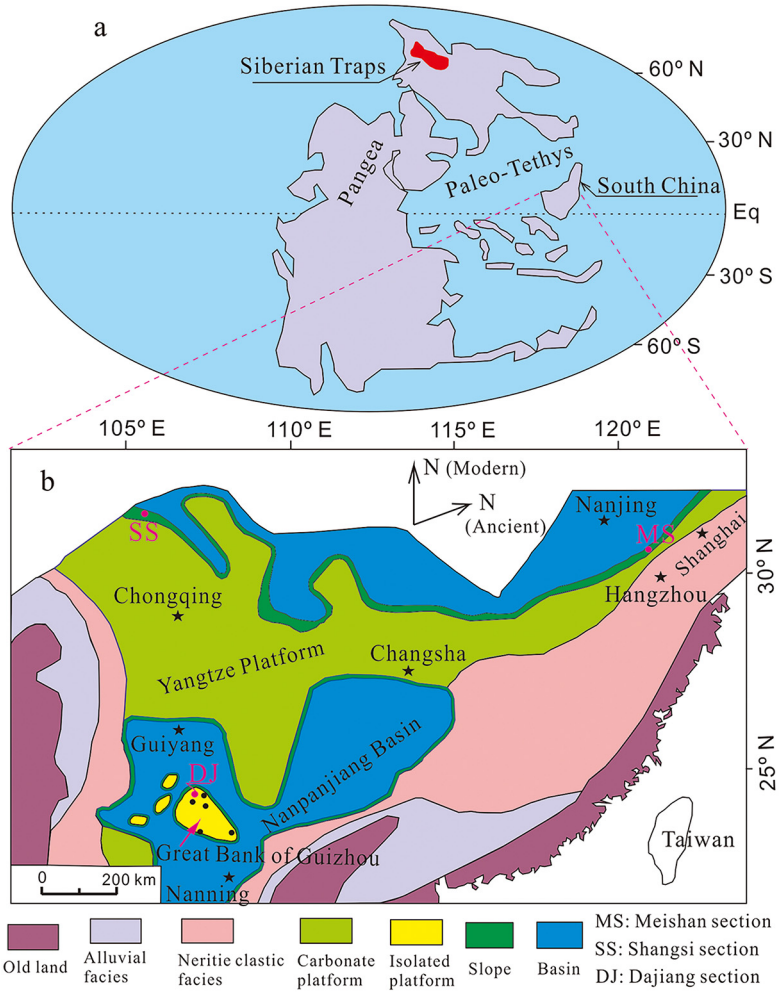

Fig. 1. (a) Paleogeography of the Paleo-Tethys Ocean and location of the South China Block during the Permian–Triassic transition (modified after Ziegler, 1988). (b) Simplified paleogeographic map of South China during the Permian–Triassic transition (modified after Yin et al., 2014).

Once the strong reaction between the carbonate and acetic acid had subsided and stabilized, the solution and residue were transferred to a 100 mL centrifuge tube, and a further 30 mL of 1.5 M acetic acid was added. The centrifuge tubes were closed and shaken with an oscillator for 24 h. Each mixture was then centrifuged to separate the supernatant from the residue. The supernatant was transferred to a 100 mL PTFE beaker and a ^{110}Cd–^{111}Cd double-spike solution (^{110}Cd/^{111}Cd ∼ 0.5; Zhang et al., 2018) was added to each sample to obtain a Cd spike to sample ratio of ∼ 2. The samples were then placed in an oscillator for 24 h to allow them to reach isotopic equilibrium. The samples were subsequently evaporated to dryness on a hot plate at 120 °C, and 5–10 mL of 2 M HCl was added to dissolve the residues. Anion exchange resin (AG-MP-1M) chromatography, as described by Zhang et al. (2018), was used to separate the Cd from the matrix. To more thoroughly remove the potential interfering elements and matrix, we re-evaporated the sample after the first purification step, dissolved the residue in 2 mL of 2 M HCl, and then undertook a second anion exchange resin (AG-MP-1M) separation step. For each batch of samples, two procedural blanks were processed to monitor the sample digestion and chemical separation techniques. In addition, two Cd secondary reference standards (Münster Cd and JMC Cd) and two geological reference materials (NOD-A-1 and NOD-P-1; Fe–Mn nodules) were processed to monitor the chemical separation and mass spectrometric techniques. The Cd contents of the procedural blanks ranged from 55 to 75 pg, which are negligible as compared with the Cd contents (> 0.10 μg) of the samples. The total Cd recovery of the chemical separation method was up to 90% for all samples. The Cd isotope ratio measurements were performed with a Neptune Plus multiple-collector (MC)–ICP–MS (Thermo Fisher Scientific; Germany) at the SKLODG. The purified Cd obtained from the samples was dissolved in 0.15 M HNO_3 for analysis by MC–ICP–MS at low resolution with Pt "Jet" sampler and Ni "x-type" skimmer cones. A Teflon nebulizer with an uptake rate of 50 μL/min was used for sample introduction. The samples were found to have Cd concentrations of ∼ 0.1 μg/mL, generally yielding a total Cd signal of 6–7 V. Each isotopic analysis consisted of two measurement sequences (i.e., runs) that were achieved by adding sub-configurations to the method. In the main run, the ion currents of ^{110}Cd, ^{111}Cd, ^{112}Cd, ^{114}Cd, and ^{117}Sn were measured simultaneously using the Faraday cups, whereas a sub-configuration (i.e., the Pd interference run) was used to determine the ion current of ^{105}Pd. The ^{105}Pd and ^{117}Sn ion beams were monitored to correct for the isobaric interferences from ^{110}Pd and ^{112}Sn–^{114}Sn, respectively. The data acquisition was carried out in 3 blocks of 20 cycles with 4.194 s integration periods during the main run, and 3 blocks of 20 cycles with 2.097 s integration periods during the Pd interference run. After each run, the sample introduction system was rinsed with 0.6 M HNO_3 until the signal intensity reached the original background level (∼ 0.05 mV of ^{111}Cd; generally af-

Table 1
Cadmium isotopic compositions and Cd contents of the samples from the Dajiang and Shangsi sections.

Dajiang section							Shangsi section						
samples	Position (cm)	Lithology	Cd (μg/g)	$\delta^{114/110}$Cd (‰)	2sd (n=3)	$\delta^{114/110}Cd_{SW}$ (‰)	samples	Position (cm)	Lithology	Cd (μg/g)	$\delta^{114/110}$Cd (‰)	2sd (n=3)	$\delta^{114/110}Cd_{SW}$ (‰)
TDJ-10	472	microbialite	0.14	+0.64	0.08	+0.77	SS-33-1	881	limestone	0.02	−0.05	0.12	+0.06
TDJ-9	312		0.15	+0.66	0.06	+0.86	SS-32-2	821		0.03	−0.20	0.10	−0.11
TDJ-8	192		0.24	+0.61	0.07	+0.77	SS-32-1	751		0.07	−0.23	0.07	−0.14
TDJ-7	142		0.31	+0.61	0.03	+0.74	SS-31-1	616		0.05	−0.07	0.06	+0.02
TDJ-6	102		0.21	+0.57	0.04	+0.76	SS-30-1	403		0.06	−0.06	0.10	+0.03
TDJ-5	62		0.34	+0.50	0.06	+0.73	SS-29-2	243	muddy limestone	0.09	−0.07	0.10	+0.06
TDJ-4	52		0.20	+0.51	0.02	+0.77	SS-28-7	147		0.05	−0.06	0.07	+0.07
TDJ-3	32		0.68	+0.77	0.03	+0.91	SS-28-6	130		0.06	−0.11	0.09	−0.01
TDJ-2	22		0.36	+0.73	0.09	+0.90	SS-28-1	2.5	calcareous mudstone	0.19	+0.24	0.02	+0.36
TDJ-1-3	12		0.30	+0.68	0.06	+0.84	SS-26-5	−1.5	limestone	0.67	+0.48	0.06	+0.68
TDJ-1-2	8		0.18	+0.61	0.06	+0.79	SS-26-4	−4.5		0.17	+0.63	0.06	+0.85
TDJ-1-1	4		0.15	+0.63	0.07	+0.82	SS-26-3	−7.5		0.17	+0.57	0.04	+0.78
PDJ-0	−2.5	packstone	0.35	+0.66	0.08	+0.81	SS-26-2	−10.5		0.25	+0.64	0.02	+0.83
PDJ-1	−5		0.32	+0.57	0.04	+0.73	SS-24-5	−38.5	siliceous limestone	0.27	+0.45	0.08	+0.58
PDJ-2	−15		0.49	+0.55	0.07	+0.73	SS-24-3	−65		0.15	+0.55	0.09	+0.68
PDJ-3	−25		0.82	+0.65	0.02	+0.82	SS-22-1	−108	limestone	0.15	+0.51	0.10	+0.61
PDJ-4	−35		0.51	+0.66	0.03	+0.89	SS-22-3	−198	siliceous limestone	0.19	+0.55	0.07	+0.69
PDJ-5	−80		0.42	+0.65	0.07	+0.91	SS-21-1	−279	limestone	0.48	+0.50	0.10	+0.63
PDJ-6	−130		0.31	+0.56	0.06	+0.82	SS-21-3	−596		0.29	+0.57	0.02	+0.69
PDJ-7	−180		0.24	+0.56	0.09	+0.75	SS-21-4	−666		0.50	+0.44	0.09	+0.56
PDJ-8	−230		0.13	+0.58	0.07	+0.88	SS-21-5	−751		0.44	+0.54	0.05	+0.67
PDJ-9	−350		0.40	+0.67	0.03	+0.92							
PDJ-10	−550		0.26	+0.64	0.10	+0.83							

$\delta^{114/110}Cd_{SW}$: The corrected Cd isotopic composition of paleo-seawater.

ter 4 min). The double-spike data reduction was performed offline using a MATLAB-based script described by Ripperger and Rehkämper (2007). The Cd isotopic compositions are reported in δ notation relative to the NIST SRM 3108 Cd solution (Abouchami et al., 2012), which is defined as follows:

$$\delta^{114/110}\mathrm{Cd}(‰) = [(^{114}\mathrm{Cd}/^{110}\mathrm{Cd})_{\mathrm{sample}}/(^{114}\mathrm{Cd}/^{110}\mathrm{Cd})_{\mathrm{NIST}} - 1] \times 1000.$$

The $\delta^{114/110}$Cd values of the four Cd reference standards used in this study, which were prepared to monitor the chemical separation and mass spectrometry measurements, are listed in Table S1.

We used the Y/Ho ratio as a proxy of paleo-salinity to estimate the $\delta^{114/110}$Cd values of paleo-seawater. Experiments have shown that the isotopic fractionation factor for Cd between calcite ($\alpha_{CaCO3-Cd(aq)}$) and seawater is 0.99955 ± 0.00012, but that there is no or minor Cd isotopic fractionation in freshwater (Horner et al., 2011). It is thus reasonable to assume that the isotopic fractionation of Cd into carbonate phases was controlled by the water salinity. In modern estuarine mixing environments, shale-normalized Y/Ho ratios vary from 0.97 for river water to 2.96 for seawater (Lawrence and Kamber, 2006). Based on the Y/Ho ratios of the marine carbonate samples, we estimated the Cd isotopic compositions of paleo-seawater ($\delta^{114/110}Cd_{SW}$) during carbonate deposition as follows (Hohl et al., 2016):

$$\delta^{114/110}\mathrm{Cd_{sw}} = \delta^{114/110}\mathrm{Cd_{sample}} + 0.45 \times [(\mathrm{Y_N}/\mathrm{Ho_N})_{\mathrm{sample}} - 0.97]/(2.96 - 0.97).$$

4. Results

The major and trace element, and Cd isotopic compositions of the Meishan section samples are from Zhang et al. (2018) (Tables S2–S3). The results for the Dajiang and Shangsi sections are described below.

4.1. Major and trace elements

The major and trace element data for the Dajiang and Shangsi sections are listed in Tables 1 and S4–S5. For the Dajiang section, the Cd, Al, $CaCO_3$, S, and total organic carbon (TOC) concentrations are 0.13–0.82 μg/g, 0.01–0.16 wt.%, 80.5–92.3 wt.%, 0.01–0.09 wt.%, and 0.10–0.31 wt.%, respectively. The Y/Ho (shale-normalized), Mn/Sr, and Cd/P ($\times 10^3$) ratios of the samples are 1.56–2.32, 0.11–0.48, and 2.2–17.5, respectively. For the Shangsi section, the Cd, Al, $CaCO_3$, S, and TOC concentrations are 0.02–0.67 μg/g, 0.28–3.93 wt.%, 38.4–83.8 wt.%, 0.03–0.98 wt.%, and 0.11–0.98 wt.%, respectively. The Y/Ho (shale-normalized), Mn/Sr, and Cd/P ($\times 10^3$) ratios are 1.36–1.94, 0.12–1.97, and 0.16–1.92, respectively.

4.2. Cadmium isotopic compositions

The Cd isotopic compositions of the Dajiang and Shangsi sections are listed in Table 1. In the three sections, the trends of the $\delta^{114/110}$Cd values (i.e., measured values) obtained from the carbonate samples are consistent with those of the paleo-seawater $\delta^{114/110}Cd_{SW}$ values (i.e., corrected values) (Fig. 2). In the following, $\delta^{114/110}Cd_{SW}$ values are discussed.

Cadmium isotopic compositions of the shallow-water section: The Cd isotopic compositions of seawater ($\delta^{114/110}Cd_{SW}$) obtained from the Dajiang section vary from +0.73‰ to +0.92‰, with an average of +0.82‰. $\delta^{114/110}Cd_{SW}$ values before the mass extinction range from +0.73‰ to +0.92‰, with an average of +0.83‰. $\delta^{114/110}Cd_{SW}$ values during and after the mass extinction vary from +0.73‰ to +0.91‰, with an average of +0.81‰. There was no significant variation in $\delta^{114/110}Cd_{SW}$ values before/after the mass extinction in the shallow-water Dajiang section (Fig. 2c).

Cadmium isotopic compositions of the deep-water sections: $\delta^{114/110}Cd_{SW}$ values of the Shangsi section vary from −0.14‰ to +0.85‰. $\delta^{114/110}Cd_{SW}$ values before the mass extinction range from +0.56‰ to +0.85‰, with an average of +0.69‰. After the mass extinction, $\delta^{114/110}Cd_{SW}$ values vary from −0.14‰ to +0.07‰, with an average of 0.00‰. The variations in $\delta^{114/110}Cd_{SW}$ values in the Shangsi section are consistent with those in the Meishan section, as reported by Zhang et al. (2018). In the relatively

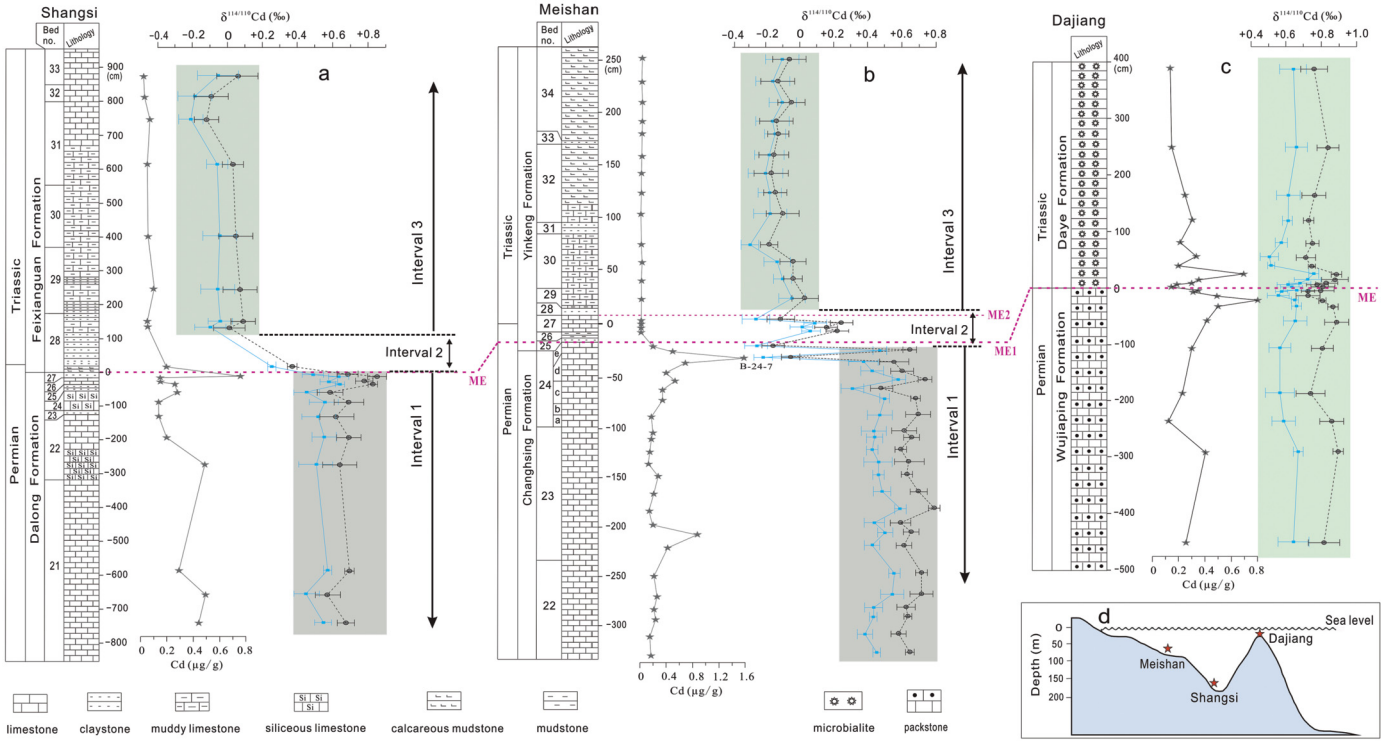

Fig. 2. Stratigraphic and $\delta^{114/110}$Cd variations in the Shangsi, Meishan, and Dajiang sections. The solid blue lines are the measured $\delta^{114/110}$Cd values of the carbonates, and the dashed lines are the salinity-corrected $\delta^{114/110}$Cd values of paleo-seawater. In (a) and (c), the lines marked ME indicate the starting horizon of the mass extinction event (Jiang et al., 2014; Godbold et al., 2017). The Cd contents and $\delta^{114/110}$Cd of the Meishan section are from Zhang et al. (2018). The lines marked ME1 and ME2 indicate the starting horizons of the two episodes of the mass extinction (Song et al., 2013).

deep-water Meishan and Shangsi sections, $\delta^{114/110}Cd_{SW}$ values were high and stable before the mass extinction, and decreased significantly during and after the extinction (Fig. 2a–b).

5. Discussion

5.1. Data evaluation and reliability

In the three sections, the strata before the mass extinction consist mainly of limestone and, after the mass extinction, are mainly limestone and calcareous mudstone. As such, it is important to evaluate the Cd isotope variations between the different lithologies. In the Dajiang section, all the samples are almost pure limestone (Fig. 2c), and Cd isotopic fractionations between different lithologies do not occur in this section. For the Meishan section, the $\delta^{114/110}$Cd values decrease abruptly in bed 24e despite the similar lithologies from bed 22 to bed 24e (Fig. 2b), suggesting that the lithology does not control the Cd isotopic variations in this section. In the Shangsi section, some beds deposited after the mass extinction consist of almost pure limestone, such as samples SS-30-1, SS-31-1, SS-32-1, SS-32-2, and SS-33-1, and their lithology is the same as those deposited before the mass extinction. However, the $\delta^{114/110}$Cd values of these five samples (−0.05‰ to −0.23‰; average = −0.12‰) are lower than those deposited before the mass extinction (+0.44‰ to +0.64‰; average = +0.54‰) (Table 1). In addition, the Cd contents ($r = 0.02$, $p < 0.01$) and $\delta^{114/110}$Cd values ($r = 0.08$, $p < 0.01$) display poor correlation with $CaCO_3$ contents in this section (Fig. 3). Therefore, we suggest that lithological differences are not responsible for the decrease in $\delta^{114/110}$Cd values after the mass extinction in the Shangsi section.

We now evaluate the effects of terrigenous detrital material on the $\delta^{114/110}$Cd values. Some trace metals (e.g., Mo, Cd, Cu, Co, Ni, Ba, U, and Zn) in sediments may be hosted in terrigenous detritus (Tribovillard et al., 2006). Therefore, the Cd in the marine carbonate sediments may also have been partly derived from terrigenous detrital components. Common detrital elements include Al, Ti, Zr, Th, and Sc, which are mainly of detrital origin and typically immobile during diagenesis (Tribovillard et al., 2006). A simple method to assess whether the content of a given element is dominantly controlled by the detrital flux is to plot the trace element content versus the detrital element content. For the Dajiang and Shangsi sections, the Al contents of samples display a poor correlation with Cd contents (for the Dajiang section, $r = 0.2$ and $p < 0.01$; for the Shangsi section, $r = -0.15$ and $p < 0.01$) (Fig. 4). This indicates that Cd was not sourced from a terrigenous detrital component.

We now evaluate the effects of biologically sourced Cd on the $\delta^{114/110}$Cd values. A small amount of Cd can be incorporated directly into carbonate rocks in organic matter, and this Cd is isotopically lighter than seawater (Lacan et al., 2006; Horner et al., 2013). The effect of the organic matter in the samples can be assessed using the TOC contents (Georgiev et al., 2015). For the samples from the Dajiang section, the Cd contents ($r = 0.17$, $p < 0.01$) and $\delta^{114/110}$Cd values ($r = 0.12$, $p < 0.01$) display a poor correlation with the TOC contents and, for the samples from the Shangsi section, the Cd contents exhibit a poor correlation ($r = -0.11$, $p < 0.01$) with the TOC contents (Fig. 5a–b and d). Although all 21 samples from the Shangsi section exhibit a weak negative correlation ($r = -0.46$, $p = 0.02$) between $\delta^{114/110}$Cd values and TOC contents, we note the following observations: (1) irrespective of whether the TOC contents are high or low, the $\delta^{114/110}$Cd values of the samples before the mass extinction are high; (2) the 13 samples with similar TOC contents, including 5 samples before the mass extinction and 8 samples after the mass extinction, exhibit a decrease in $\delta^{114/110}$Cd values after the mass extinction; and (3) the main factor associated with lower $\delta^{114/110}$Cd values is deposition after the mass extinction (Fig. 5c). Therefore, we suggest that Cd derived from organic

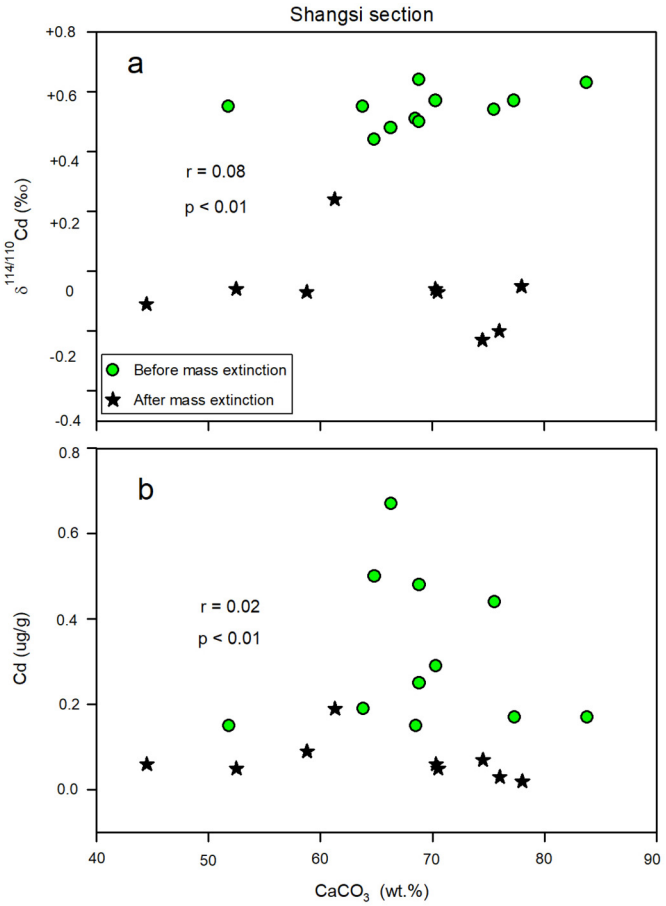

Fig. 3. Plots of $CaCO_3$ contents versus Cd contents and $\delta^{114/110}$Cd values for the Shangsi section samples.

matter has no effect on the Cd isotopic composition of the studied marine carbonate rocks.

Finally, we assess the effects of CdS precipitation on the $\delta^{114/110}$Cd values. Janssen et al. (2014) suggested that Cd (CdS) in sulfidic micro-environments in oxygen-deficient waters (<75 μmol/kg) is one of the primary mechanisms of Cd delivery to marine sediments. Evidence of CdS precipitation in oxygen-deficient seawater includes: (1) an observed deficit in dissolved Cd relative to dissolved PO_4^{3-}; (2) high particulate Cd concentrations that are not associated with high concentrations of particulate biological PO_4^{3-}; and (3) lighter particulate $\delta^{114/110}$Cd values than for dissolved Cd in the mixed layer (Janssen et al., 2014; Conway and John, 2015). When this process occurs, the CdS precipitate has a relatively high Cd/P ratio and a low $\delta^{114/110}$Cd value (Zhang et al., 2018). However, for samples from the Dajiang section, there is a poor correlation ($r = 0.11$, $p < 0.01$) between Cd/P ratios and $\delta^{114/110}$Cd values, and also a poor correlation ($r = 0.02$, $p < 0.01$) between Cd and S contents. For samples from the Shangsi section, the Cd/P ratios and $\delta^{114/110}$Cd values exhibit a moderate positive correlation ($r = 0.74$, $p < 0.01$), and the Cd and S contents exhibit a weak negative correlation ($r = -0.46$, $p = 0.03$) (Fig. 6). These correlations are opposite to those expected if Cd in seawater precipitated mainly as CdS. Therefore, we suggest that CdS removal did not affect the data from the Dajiang and Shangsi sections.

In addition, some samples from the Dajiang and Shangsi sections before and after the mass extinction show that the carbonate-phase Cd contents account for 78%–95% (average = 87%) of the total Cd in the samples (Fig. 7; Table S6). This also supports the conclusion that the Cd in the samples is mainly derived from paleo-seawater, and the amount of Cd from detrital, biological, and sulfidic sources is negligible.

In a previous study of the Meishan section (Zhang et al., 2018), the low Cd contents (0.013–0.028 μg/g) meant it was not possible to determine whether the Cd in these samples (B-29-1 to B-34-5) was mainly derived from paleo-seawater. In the present study, we analyzed the carbonate-phase Cd contents and $\delta^{114/110}$Cd values of the carbonate-phase Cd from samples B-29-1 to B-34-5. The results show that the carbonate-phase Cd contents account for 77%–96% (average = 84%) of the total Cd contents of the samples, and that the $\delta^{114/110}$Cd values of the carbonate-phase Cd are within error of those of the bulk samples reported by Zhang et al. (2018) (Table S7). Therefore, the Cd in these samples was mainly derived from paleo-seawater, and the $\delta^{114/110}$Cd values of these samples represent those of paleo-seawater.

Changes in seawater redox conditions may cause variations in the $\delta^{114/110}$Cd values of sediments. Given that Cd occurs only as Cd(II) in the natural environment, $\delta^{114/110}$Cd values are unlikely to be affected by redox reactions. However, under euxinic conditions, Cd readily forms insoluble complexes with S, during which the lighter Cd isotopes are preferentially incorporated into sulfides (CdS), resulting in the enrichment of heavier Cd isotopes in seawater (Janssen et al., 2014; Conway and John, 2015; Guinoiseau et al., 2018). The negative $\delta^{114/110}$Cd excursions in the pre- and post-extinction samples in the three studied sections do not indicate that the $\delta^{114/110}$Cd variations were caused by the formation of Cd sulfides. In addition, the lack of clear correlations (for the Dajiang section, $p = 0.49$ [>0.05] and $r = 0.52$; for the Meishan section, $p < 0.01$and $r = 0.16$) between $\delta^{114/110}$Cd values and redox proxies (e.g., $\delta^{98/95}$Mo) also precludes an effect from seawater redox conditions (Fig. S1).

5.2. Cadmium isotopic tracing of nutrient utilization and primary productivity

The nutrient concentrations and their isotope compositions of a water mass are a function of two variables—demand and supply (Farmer et al., 2021; Horner et al., 2021). Cadmium is an important nutrient element in organisms, and isotopically lighter Cd is preferentially enriched in organisms relative to seawater. As such, more Cd uptake by phytoplankton can produce seawater with higher $\delta^{114/110}$Cd values. Horner et al. (2021) proposed an Isotope Reactor Model to explain the isotopic signatures of nutrient elements (e.g., Cd), and found that if the Cd supply does not decrease, high $\delta^{114/110}$Cd values reflect high nutrient utilization and primary productivity, and if the Cd supply does not increase, low $\delta^{114/110}$Cd values reflect low nutrient utilization and primary productivity.

In modern surface ocean, Cd is mainly sourced from the upwelling of deep seawaters (e.g., Xue et al., 2013; Abouchami et al., 2014; Georgiev et al., 2015; Sieber et al., 2019), terrestrial Cd only accounts for ~10% of the amount of Cd sourced from the upwelled deep water (Martin and Thomas, 1994), and a variation of terrestrial Cd inputs is unlikely to cause an obvious change in Cd supply to marine phytoplankton. Variations in upwelling can be traced using the N isotopic composition (δ^{15}N) of marine sediments. Sediments formed in an area of weak upwelling and water-column denitrification have low δ^{15}N values (e.g., Georgiev et al., 2015; Ge and Bond, 2022; Du et al., 2023). According to previous studies, δ^{15}N values of samples from deep-water sections (Meishan and Shangsi; Cao et al., 2009; Xiang et al., 2016) and shallow-water sections (Taiping and Zuodeng; Luo et al., 2011) decreased during and after the extinction (Fig. 8b), indicative of weakened upwelling in South China. In addition, the Cd contents of the carbonate samples formed during and after the extinction also decreased com-

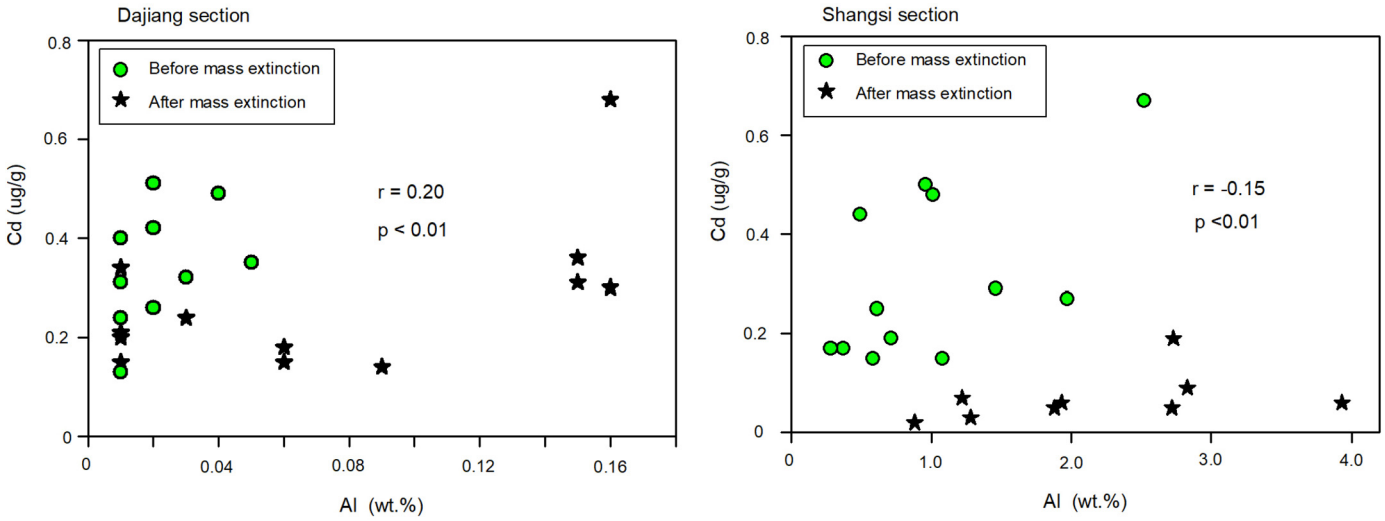

Fig. 4. Plots of Al versus Cd contents for the Dajiang and Shangsi section samples.

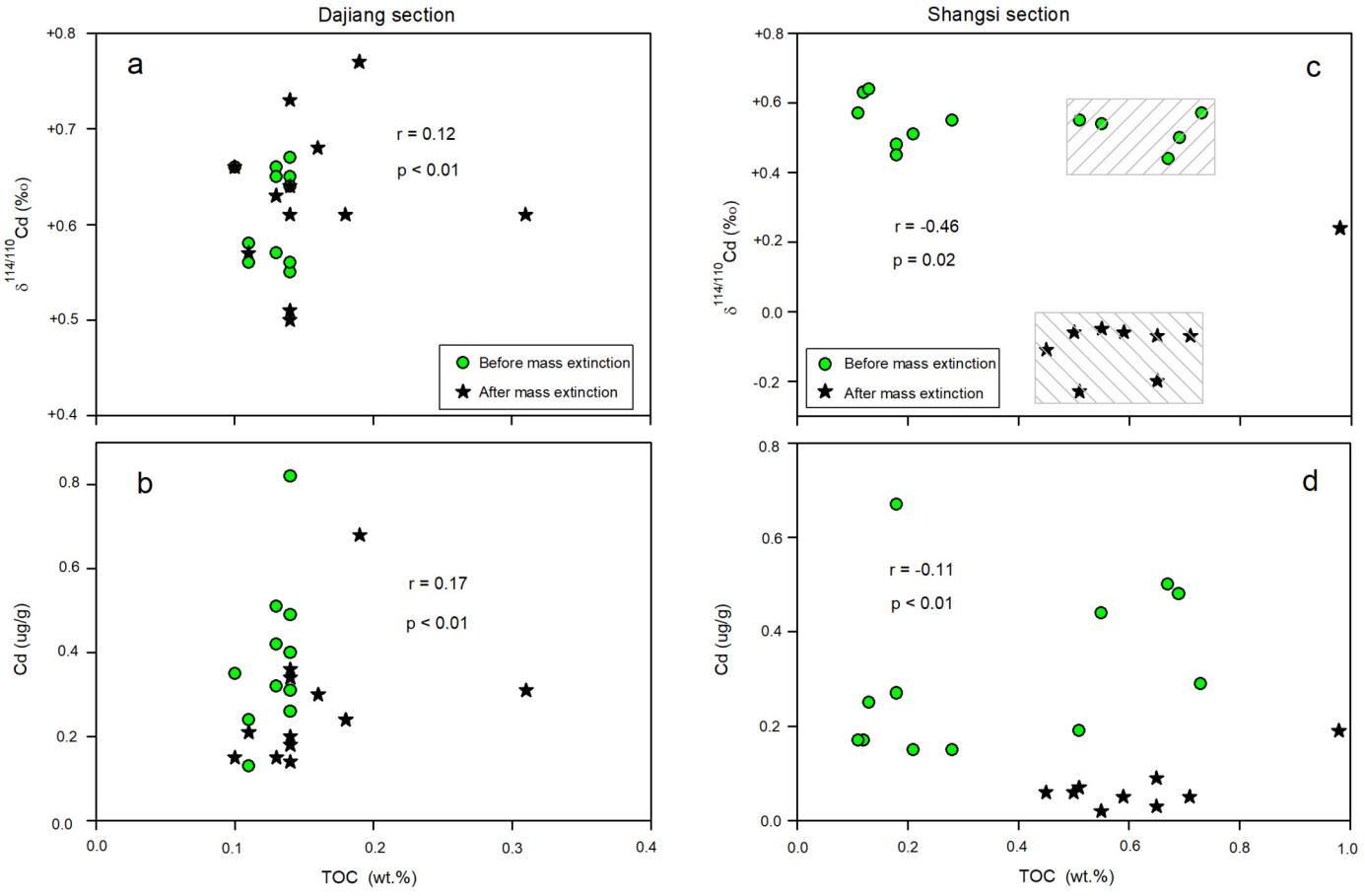

Fig. 5. Plots of TOC versus Cd contents and $\delta^{114/110}$Cd values for the Dajiang and Shangsi section samples.

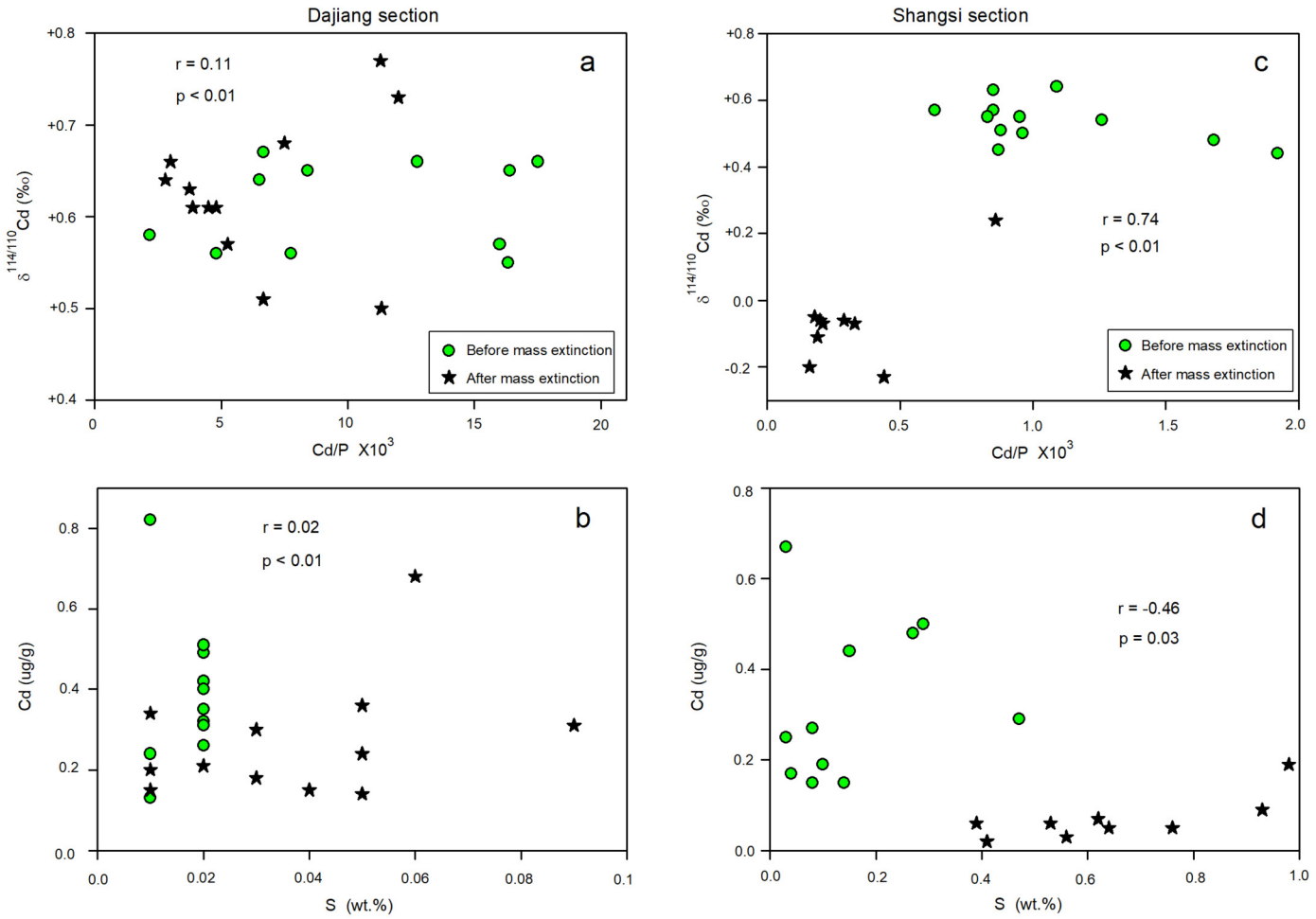

Fig. 6. Plots of (a) Cd/P versus $\delta^{114/110}$Cd and (b) S versus Cd contents for the Dajiang section samples. Plots of (c) Cd/P versus $\delta^{114/110}$Cd and (d) S versus Cd contents for the Shangsi section samples.

pared with those formed before the extinction (Fig. 8b), suggesting upwelling was an important factor that resulted in variations in Cd supply during deposition of the Meishan and Shangsi sections. Some nutrient element contents in carbonate samples from the Dajiang section exhibit no significant variations, such as for Cd, P, Fe, Zn, Cu, Co, Mn, and Sr (Fig. 8a), suggesting that the supply of these elements in shallow waters did not change before and after the extinction. In deep waters (i.e., the Meishan and Shangsi sections), the decreased upwelling resulted in a lower Cd supply. However, the nutrient utilization in the Meishan and Shangsi sections also decreased, based on the decreasing $\delta^{114/110}Cd_{SW}$ values. The mass balance between Cd supply and demand in the relatively deep waters resulted in no variations in Cd supply in the shallow waters (i.e., the Dajiang section).

In the Meishan and Shangsi sections, samples formed during and after the extinction have low $\delta^{114/110}Cd_{SW}$ values and Cd supply, which reflect low nutrient utilization and low primary productivity compared with before the extinction. In the Dajiang section, no significant variations in $\delta^{114/110}Cd_{SW}$ values and Cd supply occurred before and after the extinction, suggesting there were no or little variations in nutrient utilization and primary productivity in shallow waters.

5.3. High nutrient utilization prior to the mass extinction in the Paleo-Tethys Ocean

In the modern surface ocean, biological uptake of lighter Cd isotopes results in higher $\delta^{114/110}$Cd values in surface seawater (typically 0.6‰ – 1.0‰; e.g., Xue et al., 2013; Abouchami et al., 2014; Conway and John, 2015; George et al., 2019; Sieber et al., 2019). Prior to the mass extinction, the $\delta^{114/110}$Cd values of seawater recorded by the three studied sections were constant and high (excluding sample B-24-7 from the Meishan section, the other samples have values from +0.47‰ to +0.92‰; i.e., similar to that of modern shallow seawater), suggesting high nutrient utilization occurred prior to the mass extinction (Fig. 2). In addition, small differences were observed between the three sections. The highest $\delta^{114/110}Cd_{SW}$ values occur in the shallow-water Dajiang section (water depths < 20–30 m), whereas slightly lower $\delta^{114/110}Cd_{SW}$ values characterize the relatively deep-water sections (water depths = 50–200 m). This suggests that the nutrient utilization before the extinction was generally high, and that the utilization in the shallow-water environment was slightly higher than that in the relatively deep-water environment. The vertical distribution of nutrient utilization in the Paleo-Tethys Ocean before the end-Permian mass extinction, as indicated by the Cd isotopic data, was similar to that of the modern ocean (e.g., Ripperger et al., 2007; Abouchami et al., 2014; Conway and John, 2015; Sieber et al., 2019), suggesting the oceanic ecosystem was relatively stable before the mass extinction. The three studied sections were deposited in platform, upper slope, and lower slope environments, with seawater depths of 20–30 to 150–200 m, which suggests the nutrient utilization at ≥150 m depth was high before the mass extinction in the Paleo-Tethys Ocean.

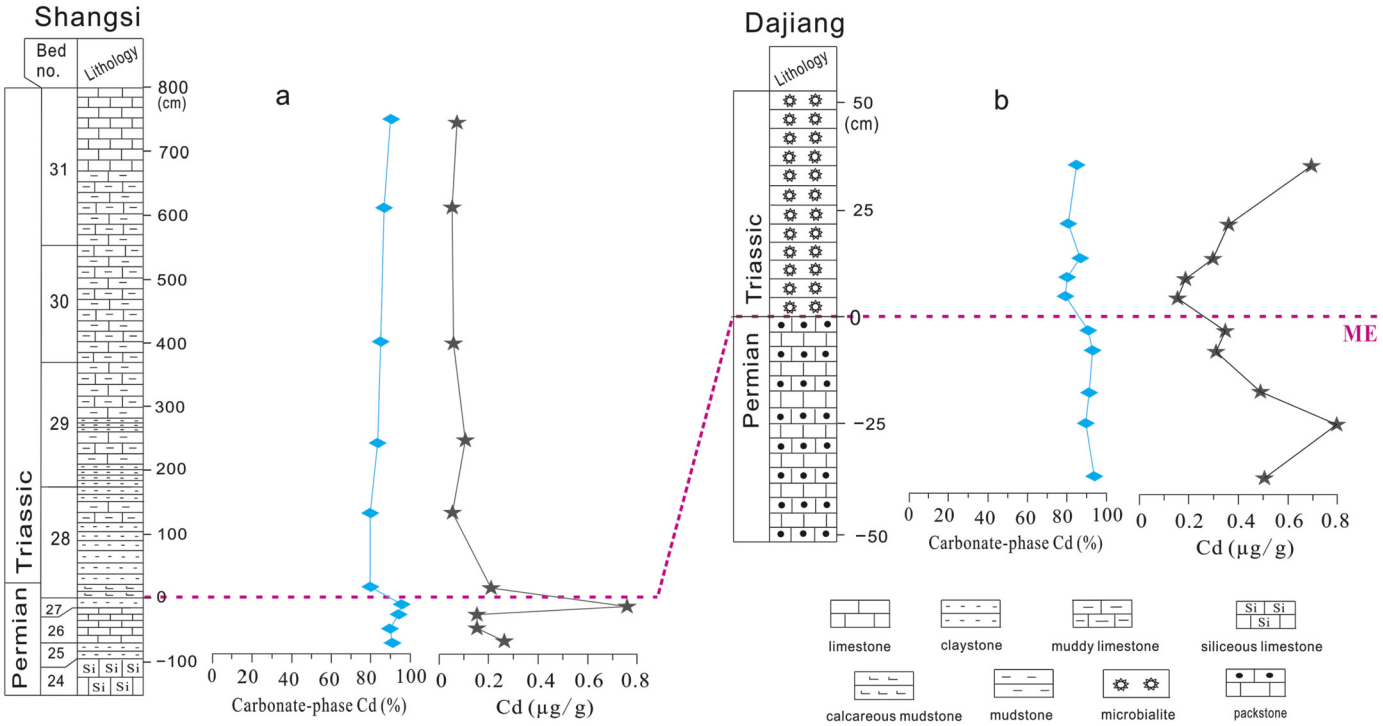

Fig. 7. The carbonate-phase Cd contents of the samples. The lines marked ME indicate the starting horizon of the mass extinction event (Jiang et al., 2014; Godbold et al., 2017).

5.4. Vertical differences in primary productivity during the mass extinction

During the mass extinction event, the $\delta^{114/110}Cd_{SW}$ values in the relatively deep-water Meishan and Shangsi sections decreased significantly, suggesting there was an abrupt decrease in the marine primary productivity. However, the changes in the primary productivities of the two sections are not completely consistent. The Meishan section exhibited fluctuations involving a decrease → increase → decrease (interval 2 in Fig. 2b), while the Shangsi section exhibited a gradual decrease (interval 2 in Fig. 2a). In the Meishan section, the decrease in primary productivity occurred before the mass extinction of macro-organisms (Zhang et al., 2018), implying that the decrease in primary productivity was one of the direct causes of the extinction of macro-organisms (i.e., a food shortage led to the mass extinction).

After the mass extinction, the $\delta^{114/110}Cd_{SW}$ values of the Meishan and Shangsi sections remain low (+0.07‰ to −0.19‰) for a long time (interval 3 in Fig. 2a–b), implying that the deep-water primary productivity, as compared with the shallow-water setting, did not recover for a long time. In detail, the observed value of −0.19‰ is considerably lighter than any Cd isotopic composition measured in the modern ocean. However, samples from the Xiaofenghe section (Ediacaran) also have negative $\delta^{114/110}Cd_{SW}$ values as low as −0.40‰ (Hohl et al., 2016). These values suggest that the Cd isotopic compositions of modern and paleo-ocean seawater are different, and further studies are needed to investigate this.

The $\delta^{114/110}Cd_{SW}$ values of the Dajiang section only exhibit small fluctuations during the mass extinction, which are negligible as compared with the analytical error (Fig. 2c). Compared with the relatively deep-water Meishan and Shangsi sections, the $\delta^{114/110}Cd_{SW}$ values of the shallow-water Dajiang section were almost constant (Fig. 2), suggesting that the decrease in marine primary productivity during the extinction event occurred mainly in deep-water settings. This is consistent with the extensive deposition of P–T boundary microbialites in shallow-water platform environments (e.g., Wang et al., 2005; Wu et al., 2016) and the occurrence of metazoan fossils in these microbialites (e.g., Forel, 2013; Yang et al., 2015; Martindale et al., 2019). In addition, in the Dajiang section, the bioclastic limestone below the extinction horizon is rich in calcareous algal fossils, which are not found in the microbialites above the extinction horizon (Song, 2012). Cyanobacteria fossils are widely distributed in the microbialites deposited above the extinction horizon (e.g., Wang et al., 2005; Wu et al., 2016). This implies that, in the shallowest platform environments, the main primary producers remaining after the extinction event were different from those present before the extinction event. It is possible that these different primary producers had slight differences in their Cd uptake capacities, but no significant Cd isotopic fractionation has been found between Chlamydomonas and Chlorella during Cd uptake in phytoplankton culturing experiments (Lacan et al., 2006). Therefore, the significant differences between the $\delta^{114/110}Cd_{SW}$ values in the Dajiang section (average = +0.81‰) and Meishan and Shangsi sections (average = −0.02‰) above the extinction horizon cannot have resulted from changes in the primary producers. We suggest that the high $\delta^{114/110}Cd_{SW}$ values in the Dajiang section during and after the mass extinction event are indicative of a high primary productivity.

5.5. Implications for the mass extinction

During the P–T transition, the marine environment was changed by several geological events (e.g., volcanic eruptions, oceanic anoxia, and ocean acidification), which resulted in >81% of marine species being eliminated and destruction of marine ecosystems (e.g., Fan et al., 2020). Our Cd isotope data indicate that the primary productivity at different seawater depths had a variable response to the changes in the marine environment. In general, the primary productivity in shallow-water settings experienced minor or no changes during the P–T transition, but this may have only been in a few extremely shallow-water areas, whereas the

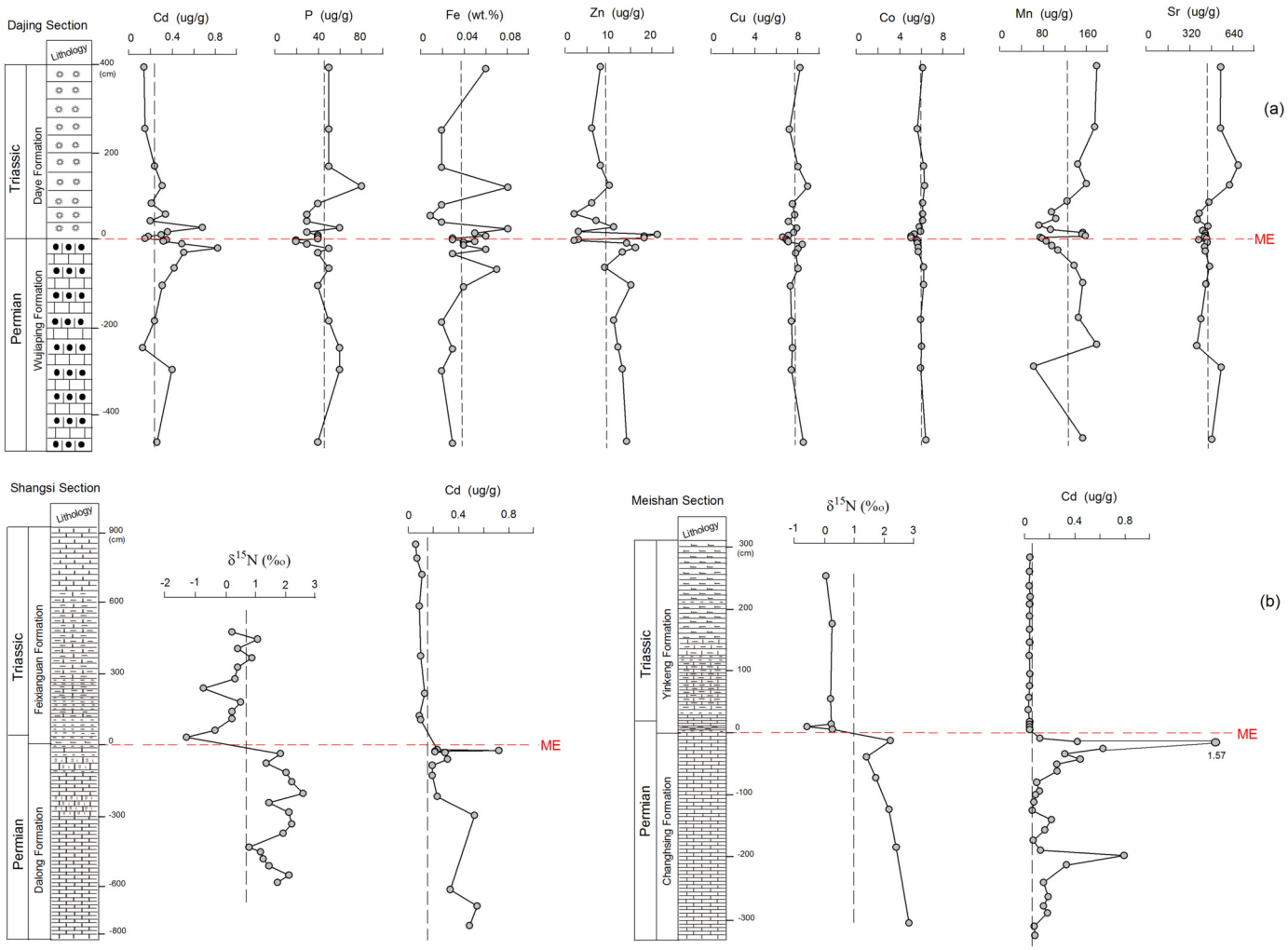

Fig. 8. (a) Stratigraphic variations of nutrient element contents in the Dajiang section, including for Cd, P, Fe, Zn, Cu, Co, Mn, and Sr. (b) Stratigraphic variations of $\delta^{15}N$ values and Cd contents in the Shangsi and Meishan sections. The $\delta^{15}N$ values for the Meishan section are from Cao et al. (2009), and the $\delta^{15}N$ values for the Shangsi section are from Xiang et al. (2016).

primary productivity over much of the relatively deep-water environments decreased significantly (Fig. 9). The vertical variations in the primary productivity indicate that the main factor responsible for the decrease in primary productivity was the change in the deep-water environment. Shen et al. (2011) suggested that episodic upwelling of sulfidic and anoxic deep seawater caused the end-Permian mass extinction, and the vertical variations in the primary productivity in the studied sections support this hypothesis. The Siberian Traps volcanism is considered to be one of the main drivers of the end-Permian mass extinction (e.g., Burgess et al., 2017; Liu et al., 2017; Shen et al., 2019; Jurikova et al., 2020), but the driving mechanisms are not well constrained. In the Meishan section, Zn isotopes indicate there was a volcanic or hydrothermal Zn source during the mass extinction (Liu et al., 2017), but Hg isotope data do not reveal the atmospheric-derived signature of volcanic Hg (Grasby et al., 2017; Wang et al., 2018). We speculate that volcanic eruptions from the Siberian Traps changed the marine environment as follows: (1) the volcanic eruptions led to a large amount of S-containing materials entering the ocean; (2) these S-containing materials were carried by ocean currents to regions far from Siberia, which resulted in the seawater in these regions gradually becoming sulfidic and anoxic; and (3) the anoxic areas gradually expanded to the surface seawater. However, undiscovered submarine volcanoes or hydrothermal fluids could have also been involved. We suggest that the anoxic and sulfidic environment was a key factor in the decline in primary productivity in relatively deep waters.

In the shallow-water platform areas, the bioclastic limestone below the extinction horizon is rich in calcareous algal fossils, but such fossils have not been found in the microbialites, which instead contain a large amount of cyanobacteria fossils (e.g., Wang et al., 2005; Song, 2012; Wu et al., 2016). This indicates that cyanobacteria may have become the main primary producer during the mass extinction. In addition, although the biological content of the microbialites is relatively high, the species are not diverse (e.g., Wang et al., 2005). Although the primary productivity of the shallow-water areas did not decrease during the extinction event, the surface seawater ecosystem was also affected by environmental stress, which may have been mainly due to the gradual expansion of deep anoxic seawater to the surface. Given that there was oxygen exchange between the surface seawater and atmosphere, the degree of anoxia was not as severe as in the deep waters. The environment in the extremely shallow-water areas was slightly more suitable for survival than in the deep-water settings. Some primary producers that were more able to adapt to extreme environments migrated to surface waters and survived, and/or some primary producers prospered that originally lived in surface waters that had

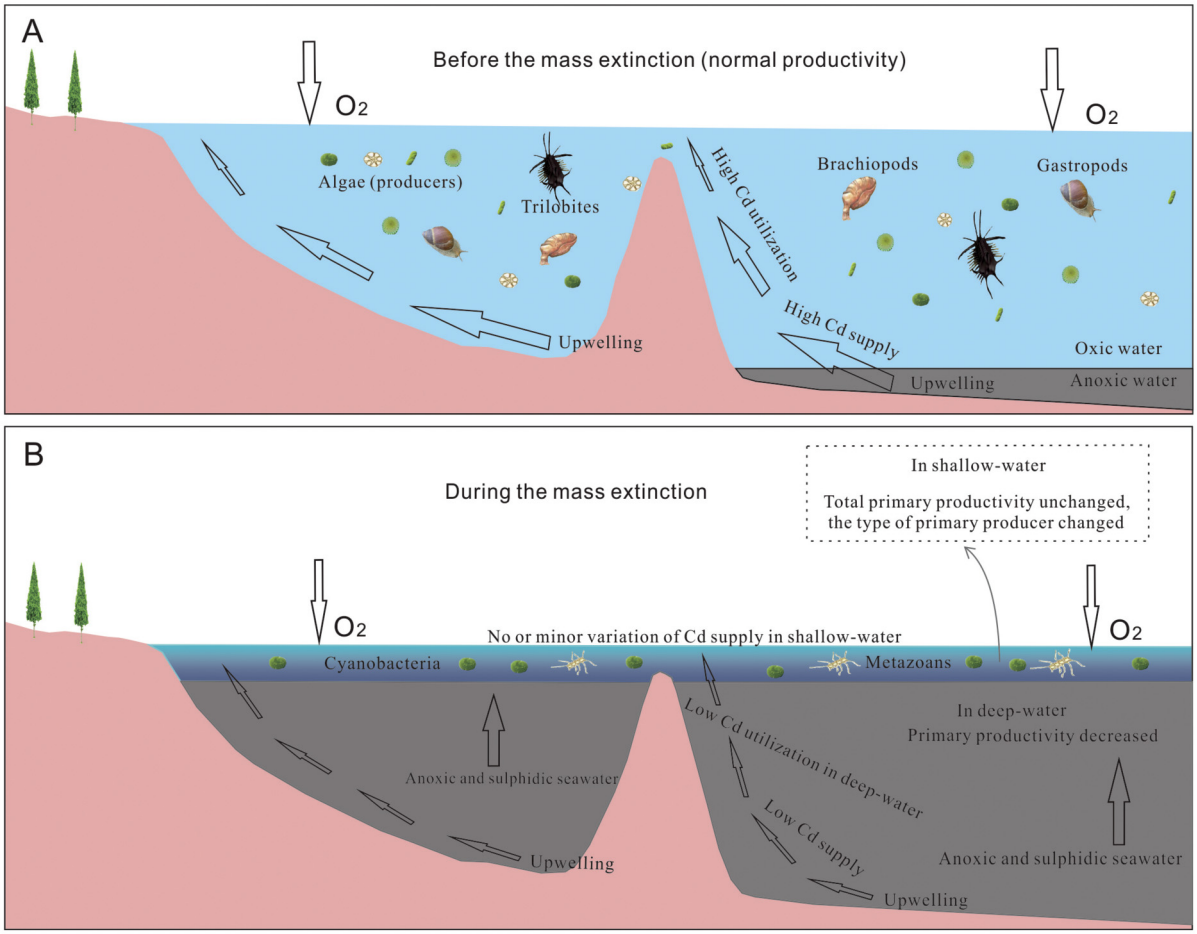

Fig. 9. Schematic diagram showing the vertical evolution of marine primary productivity during the Permian–Triassic transition.

the ability to adapt to extreme environments due to a lack of competitors.

6. Conclusions

In the late Permian, before the end-Permian mass extinction, the nutrient utilization in the Paleo-Tethys Ocean was relatively high and stable in both shallow- and deep-water settings. During the mass extinction event and Early Triassic, with the exception of extremely shallow-water platform environments, the primary productivity in relatively deep-water environments decreased significantly. The decrease in primary productivity may have been one of the causes of the destruction of deep-water marine ecosystems. In the shallow-water platform environments, although Cd isotopes indicate that there was no significant change in primary productivity before/after the extinction, the types of primary producers may have changed, and this may have contributed to the mass extinction in the shallow-water platform environments.

The vertical variations in the primary productivity in the Paleo-Tethys Ocean during the end-Permian mass extinction suggest that the environmental factors leading to extinction events mainly began in deep waters, and the upward expansion of sulfidic and anoxic deep waters is one of the causes of mass extinctions. The Siberian Traps may have been a trigger for the end-Permian mass extinction. The volcanic eruptions provided a large amount of sulfur-containing materials into the ocean, and then these sulfur-containing substances were carried to regions far from Siberia by ocean currents, resulting in sulfidic and anoxic conditions in deep waters that expanded to the surface.

CRediT authorship contribution statement

Yuxu Zhang: Writing – review & editing, Writing – original draft, Methodology, Investigation, Funding acquisition, Data curation, Conceptualization. **Hanjie Wen:** Funding acquisition, Conceptualization. **Haifeng Fan:** Writing – review & editing. **Chuanwei Zhu:** Writing – review & editing. **Jiafei Xiao:** Investigation. **Pan Qiao:** Data curation.

Declaration of competing interest

The authors declare no competing interests.

Data availability

Data will be made available on request.

Acknowledgements

This research was financially supported by the National Natural Science Foundation of China (Grant Nos. 92162214, 92062221, 41573007, 41773015, and U1812402) and the Key R&D Program of Yunnan Province (202103AQ100003).

Appendix A. Supplementary material

Supplementary material related to this article can be found online at https://doi.org/10.1016/j.epsl.2023.118371.

References

Abouchami, W., Galer, S.J.G., de Baar, H.J.W., Alderkamp, A.C., Middag, R., Laan, P., Feldmann, H., Andreae, M.O., 2011. Modulation of the Southern Ocean cadmium isotope signature by ocean circulation and primary productivity. Earth Planet. Sci. Lett. 305 (1–2), 83–91.

Abouchami, W., Galer, S.J.G., de Baar, H.J.W., Middag, R., Vance, D., Zhao, Y., Klunder, M., Mezger, K., Feldmann, H., Andreae, M.O., 2014. Biogeochemical cycling of cadmium isotopes in the Southern Ocean along the Zero Meridian. Geochim. Cosmochim. Acta 127 (3), 348–367.

Abouchami, W., Galer, S.J.G., Horner, T.J., Rehkämper, M., Wombacher, F., Xue, Z.C., Lambelet, M., Gault-Ringold, M., Stirling, C.H., Schönbächler, M., Shiel, A.E., Weis, D., Holdship, P.F., 2012. A common reference material for cadmium isotope studies - NIST SRM 3108. Geostand. Geoanal. Res. 37, 5–17.

Bewers, J.M., Yeats, P.A., 1977. Oceanic residence times of trace-metals. Nature 268, 595–598.

Boyle, E.A., Sclater, F., Edmond, J.M., 1976. On the marine geochemistry of cadmium. Nature 263, 42–44.

Burgess, S.D., Muirhead, J.D., Bowring, S.A., 2017. Initial pulse of Siberian Traps sills as the trigger of the end-Permian mass extinction. Nat. Commun. 8, 164.

Cao, C.Q., Love, G.D., Hays, L.E., Wang, W., Shen, S.Z., Summons, R.E., 2009. Biogeochemical evidence for euxinic oceans and ecological disturbance presaging the end-Permian mass extinction event. Earth Planet. Sci. Lett. 281, 188–201.

Conway, T.M., John, S.G., 2015. Biogeochemical cycling of cadmium isotopes along a high-resolution section through the North Atlantic Ocean. Geochim. Cosmochim. Acta 148, 269–283.

de Baar, H.J.W., Saager, P.M., Nolting, R.F., der Meer, J.V., 1994. Cadmium versus phosphate in the world ocean. Mar. Chem. 46, 261–281.

Druce, M., Stirling, C.H., Bostock, H.C., Rolison, J.M., 2022. Cadmium isotope systematics in sedimentary carbonate: extending the utility of the cadmium isotope palaeo-productivity proxy. Geochim. Cosmochim. Acta 339, 80–96.

Du, Y., Song, H.Y., Grasby, S.E., Xing, T., Song, H.J., Tian, L., Chu, D.L., Wu, Y.Y., Corso, J.D., Algeo, T.J., Tong, J.N., 2023. Recovery from persistent nutrient-N limitation following the Permian–Triassic mass extinction. Earth Planet. Sci. Lett. 602, 117944.

Fan, J.X., Shen, S.Z., Erwin, D.H., Sadler, P.M., Macleod, N., Cheng, Q.M., Hou, X.D., Yang, J., Wang, X.D., Wang, Y., Zhang, H., Chen, X., Li, G.X., Zhang, Y.C., Shi, Y.K., Yuan, D.X., Chen, Q., Zhang, L.N., Li, C., Zhao, Y.Y., 2020. A high-resolution summary of Cambrian to Early Triassic marine invertebrate biodiversity. Science 367, 272–277.

Farmer, J.R., Hertzberg, J.E., Cardinal, D., Fietz, S., Hendry, K., Jaccard, S.L., Paytan, A., Rafter, P.A., Ren, H., Somes, C.J., Sutton, J.N., Members, G.P.B.P.W.G., 2021. Assessment of C, N, and Si isotopes as tracers of past ocean nutrient and carbon cycling. Glob. Biogeochem. Cycles 35, e2020GB006775.

Field, C.B., Behrenfeld, M.J., Randerson, J.T., Falkowski, P., 1998. Primary production of the biosphere: integrating terrestrial and oceanic components. Science 281 (5374), 237.

Forel, M.B., 2013. The Permian–Triassic mass extinction: Ostracods (Crustacea) and microbialites. C. R. Géosci. 345, 203–211.

Frederiksen, J.A., Wei, W., Rugen, E.J., Ling, H.F., Frei, R., 2022. Cadmium isotopes in Late Ediacaran–Early Cambrian Yangtze Platform carbonates – reconstruction of bioproductivity in ambient surface seawater. Palaeogeogr. Palaeoclimatol. Palaeoecol. 601, 111096.

Garbelli, C., Angiolini, L., Shen, S.Z., 2017. Biomineralization and global change: a new perspective for understanding the end-Permian extinction. Geology 45 (1), 19–22.

Ge, Y.Z., Bond, D.P.G., 2022. Two deep marine oxygenation events during the Permian-Triassic boundary interval in South China: relationship with ocean circulation and marine primary productivity. Earth-Sci. Rev. 234, 104220.

George, E., Stirling, C.H., Gault-Ringold, M., Ellwood, M.J., Middag, R., 2019. Marine biogeochemical cycling of cadmium and cadmium isotopes in the extreme nutrient-depleted subtropical gyre of the South West Pacific Ocean. Earth Planet. Sci. Lett. 514, 84–95.

Georgiev, S.V., Horner, T.J., Stein, H.J., Hannah, J.L., Bingen, B., Rehkämper, M., 2015. Cadmium-isotopic evidence for increasing primary productivity during the Late Permian anoxic event. Earth Planet. Sci. Lett. 410, 84–96.

Godbold, A., Schoepfer, S., Shen, S.Z., Henderson, C.M., 2017. Precarious ephemeral refugia during the earliest Triassic. Geology 45 (7), 607–610.

Grasby, S.E., Beauchamp, B., Knies, J., 2016. Early Triassic productivity crises delayed recovery from world's worst mass extinction. Geology 44 (9), 779–782.

Grasby, S.E., Shen, W.J., Yin, R.S., Gleason, J.D., Blum, J.D., Lepak, R.F., Hurley, J.P., Beauchamp, B., 2017. Isotopic signatures of mercury contamination in latest Permian oceans. Geology 45 (1), 55–58.

Grice, K., Cao, C.Q., Love, G.D., Bottcher, M.E., Twitchett, R.J., Grosjean, E., Summons, R.E., Turgeon, S.C., Dunning, W., Jin, Y.G., 2005. Photic zone euxinia during the Permian-Triassic superanoxic event. Science 307, 706–709.

Guinoiseau, D., Galer, S.J.G., Abouchami, W., 2018. Effect of cadmium sulphide precipitation on the partitioning of Cd isotopes: implications for the oceanic Cd cycle. Earth Planet. Sci. Lett. 498, 300–308.

Hohl, S.V., Galer, S.J.G., Gamper, A., Becker, H., 2016. Cadmium isotope variations in Neoproterozoic carbonates–a tracer of biologic production? Geochem. Perspect. Lett. 3, 32–44.

Horner, T.J., Rickaby, R.E.M., Henderson, G.M., 2011. Isotopic fractionation of cadmium into calcite. Earth Planet. Sci. Lett. 312, 243–253.

Horner, T.J., Lee, R.B.Y., Henderson, G.M., Rickaby, R.E.M., 2013. Nonspecific uptake and homeostasis drive the oceanic cadmium cycle. Proc. Natl. Acad. Sci. USA 110 (7), 2500–2505.

Horner, T.J., Little, S.H., Conway, T.M., Farmer, J.R., Hertzberg, J.E., Janssen, D.J., Lough, A.J.M., McKay, J.L., Tessin, A., Galer, S.J.G., Jaccard, S.L., Lacan, F., Paytan, A., Wuttig, K., Members, G.P.B.P.W.G., 2021. Bioactive trace metals and their isotopes as paleoproductivity proxies: an assessment using GEOTRACES-Era data. Glob. Biogeochem. Cycles 35, e2020GB006814.

Janssen, D.J., Conway, T.M., John, S.G., Christian, J.R., Kramer, D.I., Pedersen, T.F., Cullen, J.T., 2014. Undocumented water column sink for cadmium in open ocean oxygen-deficient zones. Proc. Natl. Acad. Sci. USA 111 (19), 6888–6893.

John, S.G., Kunzmann, M., Townsend, E.J., Rosenberg, A.D., 2017. Zinc and cadmium stable isotopes in the geological record: a case study from the post-snowball Earth Nuccaleena cap dolostone. Palaeogeogr. Palaeoclimatol. Palaeoecol. 466, 202–208.

Jiang, H.S., Lai, X.L., Sun, Y.D., Wignall, P.B., Liu, J.B., Yan, C.B., 2014. Permian–Triassic Conodonts from Dajiang (Guizhou, South China) and their implication for the age of microbialite deposition in the Aftermath of the end-Permian mass extinction. J. Earth Sci. 25 (3), 413–430.

Jurikova, H., Gutjahr, M., Wallmann, K., Flögel, S., Liebetrau, V., Posenato, R., Angiolini, L., Garbelli, C., Brand, U., Wiedenbeck, M., Eisenhauer, A., 2020. Permian-Triassic mass extinction pulses driven by major marine carbon cycle perturbations. Nat. Geosci. 13, 745–750.

Lacan, F., Francois, R., Ji, Y.C., Sherrell, R.M., 2006. Cadmium isotopic composition in the ocean. Geochim. Cosmochim. Acta 70, 5104–5118.

Lane, T.W., Saito, M.A., George, G.N., Pickering, I.J., Prince, R.C., Morel, F.M.M., 2005. A cadmium enzyme from a marine diatom. Nature 435, 42.

Lawrence, M.G., Kamber, B.S., 2006. The behaviour of the rare earth elements during estuarine mixing-revisited. Mar. Chem. 100 (1–2), 147–161.

Lehrmann, D.J., Wei, J.Y., Enos, P., 1998. Controls on facies architecture of a large Triassic carbonate platform, the Great Bank of Guizhou, Nanpanjiang Basin, South China. J. Sediment. Res. 68 (2), 311–326.

Lei, Y., Shen, J., Algeo, T.J., Servais, T., Feng, Q.L., Yu, J.X., 2019. Phytoplankton (acritarch) community changes during the Permian-Triassic transition in South China. Palaeogeogr. Palaeoclimatol. Palaeoecol. 519, 84–94.

Liu, S.A., Wu, H.C., Shen, S.Z., Jiang, G.Q., Zhang, S.H., Lv, Y.W., Zhang, H., Li, S.G., 2017. Zinc isotope evidence for intensive magmatism immediately before the end-Permian mass extinction. Geology 45 (4), 343–346.

Luo, G.M., Wang, Y.B., Algeo, T.J., Kump, L.R., Bai, X., Yang, H., Yao, L., Xie, S.C., 2011. Enhanced nitrogen fixation in the immediate aftermath of the latest Permian marine mass extinction. Geology 39 (7), 647–650.

Martin, J.M., Thomas, A.J., 1994. The global insignificance of telluric input of dissolved trace metals (Cd, Cu, Ni and Zn) to ocean margins. Mar. Chem. 46, 165–178.

Martindale, R.C., Foster, W.J., Velledits, F., 2019. The survival, recovery, and diversification of metazoan reef ecosystems following the end-Permian mass extinction event. Palaeogeogr. Palaeoclimatol. Palaeoecol. 513, 100–115.

Meyer, K.M., Yu, M., Jost, A.B., Kelley, B.M., Payne, J.L., 2011. δ13C evidence that high primary productivity delayed recovery from end-Permian mass extinction. Earth Planet. Sci. Lett. 302, 378–384.

Paytan, A., Mclaughlin, K., 2007. The oceanic phosphorus cycle. Chem. Rev. 107 (2), 563–576.

Qiu, Z.P., Song, H.J., Hu, C.Y., Wignall, P.B., Song, H.Y., 2019. Carbonate thermoluminescence and its implication for marine productivity change during the Permian-Triassic transition. Palaeogeogr. Palaeoclimatol. Palaeoecol. 526, 72–79.

Ripperger, S., Rehkämper, M., 2007. Precise determination of cadmium isotope fractionation in seawater by double spike MC-ICPMS. Geochim. Cosmochim. Acta 71, 631–642.

Ripperger, S., Rehkämper, M., Porcelli, D., Halliday, A.N., 2007. Cadmium isotope fractionation in seawater – a signature of biological activity. Earth Planet. Sci. Lett. 261, 670–684.

Shen, J., Schoepfer, S.D., Feng, Q.L., Zhou, L., Yu, J.X., Song, H.Y., Wei, H.Y., Algeo, T.J., 2015. Marine productivity changes during the end-Permian crisis and Early Triassic recovery. Earth-Sci. Rev. 149, 136–162.

Shen, S.Z., Ramezani, J., Chen, J., et al., 2019. A sudden end-Permian mass extinction in South China. GSA Bull. 131 (1/2), 205–223.

Shen, Y.A., Farquhar, J., Zhang, H., Masterson, A., Zhang, T.G., Wing, B.A., 2011. Multiple S-isotopic evidence for episodic shoaling of anoxic water during Late Permian mass extinction. Nat. Commun. 2 (1), 116–119.

Sieber, M., Conway, T.M., de Souza, G.F., Obata, H., Takano, S., Sohrin, Y., Vance, D., 2019. Physical and biogeochemical controls on the distribution of dissolved cadmium and its isotopes in the Southwest Pacific Ocean. Chem. Geol. 511, 494–509.

Song, H.J., 2012. Extinction and recovery of foraminifera and calcareous algae during the Permian-Triassic Transition. Ph.D. thesis. China University of Geosciences, Wuhan, pp. 93–94 (in Chinese with English abstract).

Song, H.J., Wignall, P.B., Tong, J.N., Yin, H.F., 2013. Two pulses of extinction during the Permian-Triassic crisis. Nat. Geosci. 6 (1), 52–56.
Tesoriero, A.J., Pankow, J.F., 1996. Solid solution partitioning of Sr2+, Ba2+, and Cd2+ to calcite. Geochim. Cosmochim. Acta 60 (6), 1053–1063.
Tribovillard, N., Algeo, T.J., Lyons, T., Riboulleau, A., 2006. Trace metals as paleoredox and paleoproductivity proxies: an update. Chem. Geol. 232 (1–2), 12–32.
Tyrrell, T., 1999. The relative influences of nitrogen and phosphorus on oceanic primary production. Nature 400, 525–531.
Wang, Y.B., Tong, J.N., Wang, J.S., Zhou, X.G., 2005. Calcimicrobialite after end-Permian mass extinction in South China and its palaeoenvironmental significance. Chin. Sci. Bull. 50 (7), 665–671.
Wang, X.D., Cawood, P.A., Zhao, H., Zhao, L.S., Grasby, S.E., Chen, Z.Q., Wignall, P.B., Lv, Z.Y., Han, C., 2018. Mercury anomalies across the end Permian mass extinction in South China from shallow and deep water depositional environments. Earth Planet. Sci. Lett. 496, 159–167.
Wu, Y.S., Yu, G.L., Jiang, H.X., Liu, L.J., Zhao, R., 2016. Role and lifestyle of calcified cyanobacteria (Stanieria) in Permian–Triassic boundary microbialites. Palaeogeogr. Palaeoclimatol. Palaeoecol. 448, 39–47.
Xiang, L., Schoepfer, S.D., Zhang, H., Yuan, D.X., Cao, C.Q., Zheng, Q.F., Henderson, C.M., Shen, S.Z., 2016. Oceanic redox evolution across the end-Permian mass extinction at Shangsi, South China. Palaeogeogr. Palaeoclimatol. Palaeoecol. 448, 59–71.
Xue, Z.C., Rehkämper, M., Horner, T.J., Abouchami, W., Middag, R., de Flierd, T.V., de Baar, H.J.W., 2013. Cadmium isotope variations in the Southern Ocean. Earth Planet. Sci. Lett. 382, 161–172.
Yang, H., Chen, Z.Q., Wang, Y.B., Ou, W.Q., Liao, W., Mei, X., 2015. Palaeoecology of microconchids from microbialites near the Permian–Triassic boundary in South China. Lethaia 48, 497–508.
Yin, H.F., Zhang, K.X., Tong, J.N., Yang, Z.Y., Wu, S.B., 2001. The global stratotype section and point (GSSP) of the Permian-Triassic boundary. Episodes 24, 102–114.
Yin, H.F., Jiang, H.S., Xia, W.C., Feng, Q.L., Zhang, N., Shen, J., 2014. The end-Permian regression in South China and its implication on mass extinction. Earth-Sci. Rev. 137, 19–33.
Ziegler, P.A., 1988. Evolution of the Arctic-North Atlantic and the Western Tethys. Memoir 43 American Association of Petroleum Geologists. 198p.
Zhang, F.F., Shen, S.Z., Cui, Y., Lenton, T.M., Dahl, T.W., Zhang, H., Zheng, Q.F., Wang, W.Q., Krainer, K., Anbar, A.D., 2020. Two distinct episodes of marine anoxia during the Permian-Triassic crisis evidenced by uranium isotopes in marine dolostones. Geochim. Cosmochim. Acta 287, 165–179.
Zhang, H., Zhang, F.F., Chen, J.B., et al., 2021. Felsic volcanism as a factor driving the end-Permian mass extinction. Sci. Adv. 7 (47), eabh1390.
Zhang, X.Y., Zheng, Q.F., Li, Y., Yang, H.Q., Zhang, H., Wang, W.Q., Shen, S.Z., 2020. Polybessurus-like fossils as key contributors to Permian–Triassic boundary microbialites in South China. Palaeogeogr. Palaeoclimatol. Palaeoecol. 552, 109770.
Zhang, Y.X., Wen, H.J., Zhu, C.W., Fan, H.F., Cloquet, C., 2018. Cadmium isotopic evidence for the evolution of marine primary productivity and the biological extinction event during the Permian-Triassic crisis from the Meishan section, South China. Chem. Geol. 481, 110–118.
Zheng, Q.F., Zhang, H., Yuan, D.X., Wang, Y., Wang, W.Q., Cao, C.Q., Shen, S.Z., 2022. High-resolution sedimentology, ichnology, and benthic marine redox conditions from Late Permian to the earliest Triassic at Shangsi, South China: Local, regional, and global signals and driving mechanisms. Earth-Sci. Rev. 225, 103898.